Acta Geologica Sinica (English Edition), 2019, 93(5): 1580–1590

Initiation Timing of the Jiamusi–Yitong Fault Zone in NE China

WEN Quanbo[1], LIU Yongjiang[2, 3, *], LIANG Chenyue[1, 4], Li Weimin[1, 4], SHAO Yilun[5], ZHANG Qian[1], ZHANG Duo[1] and LIU Xinyue[1]

[1] *College of Earth Sciences, Jilin University, Changchun 130061, China*
[2] *Key Lab of Submarine Geosciences and Prospecting Techniques, MOE, Institute for Advanced Ocean Study, College of M arine Geosciences, Ocean University of China, Qingdao 266100, China*
[3] *Laboratory for Marine Mineral Resources, Qingdao National Laboratory for Marine Science and Technology, Qingdao 266237, China*
[4] *Key laboratory of Mineral Resources Evaluation in Northeast Asia, Ministry of Land and Resources, Changchun 130061*
[5] *Department of Geology, University of Otago, Dunedin 9016, New Zealand*

Abstract: The NE–striking Jiamusi–Yitong fault zone (JYFZ) is the most important branch in the northern segment of the Tancheng–Lujiang fault zone. The precise shearing time of its large–scale sinistral strike–slip has yet to determined and must be constrained. Detailed field investigations and comprehensive analyses show that strike–slip faults or ductile shear belts exist as origination structures along the western region of Yitong Graben. The strike of the shear belts trend to the NE–SW with steep mylonitic foliation. The zircon U–Pb dating result for the granite was 264.1±1 Ma in the ductile shear belt of the JYFZ. The microstructural observation (rotated feldspar porphyroclasts, S–C fabrics, and quartz c–axis fabrics, etc.) demonstrated the sinistral shearing of the ductile shear zones. Moreover, the recrystallized quartz types show a transitional stage of the subgrain rotation toward the recrystallization of the grain boundary migration (SR–GBM). Therefore, we suggest that the metamorphic grade of the shear zone in the ductile shear zones should have reached high greenschist facies conditions, and the deformation temperatures should approximately 450–500°C, which is obviously higher than the blocking temperature of muscovite (300–400°C). Hence, the $^{40}Ar/^{39}Ar$ isochron age of muscovite from ductile shear zones should be a cooling age (162.7±1 Ma). We infer that the sinistral strike–slipping event at the JYFZ occurred in the late Jurassic period, and it was further inferred from the ages of the main geological events in this region that the second sinistral strike–slip age of the Tancheng–Lujiang fault zone occurred during the period of tectonic movements in the Circum–Pacific tectonic domain. This discovery also indicates the age of the Tancheng–Lujiang fault zone that stretches to northeastern China. The initiation of the JYFZ in the late Jurassic is related to the speed and direction of oblique subduction of the west Pacific Plate under the Eurasian continent and is responsible for collision during the Jurassic period.

Key words: Origin structures, sinistral ductile shear belt, microstructures, $^{40}Ar/^{39}Ar$ dating, Jiamusi–Yitong Fault Zone

Citation: Wen et al., 2019. Initiation Timing of the Jiamusi–Yitong Fault Zone in NE China. Acta Geologica Sinica (English Edition), 93(5): 1580–1590. DOI: 10.1111/1755-6724.14389

1 Introduction

The NE trend of the Jiamusi–Yitong fault zone (JYFZ) is mainly distributed along the Jiamusi–Shulan–Yitong–Tieling belt in China and stretches to Russia to the north (Fig. 1). Combined with the Dunhua–Mishan fault zone (or Dun–Mi fault zone), the two major fault zones are believed to be the largest fault zones, which are together called the Tancheng–Lujiang fault zone (or Tan–Lu fault zone) in Eastern China (Zhang et al., 1995; Wang et al., 1997; Zhang et al., 1999; Zhu et al., 2002; Zhang et al., 2005). The heavy vegetation in the fault zone seriously restricts study; thus, the degree of geological studies of this area is apparently lower than for the middle and southern part of the Tan–Lu fault zone in different aspects (geometric features, kinematic features, divisions of the tectonics evolution stage, and the determination of the fracture mechanic properties of different tectonic evolution stages).

Currently, studies of the formation time of the Tan–Lu fault zone are mainly focused on the middle and southern regions. Most researchers have indicated that the middle and southern part of the Tan–Lu fault zone formed in the middle Triassic period (Chen et al., 2000; Zhang et al., 2008; Zhao et al., 2016), and sinistral strike–slip movement again occurred in the late Mesozoic (Xu et al., 1987; Zhu et al., 2005; Wang, 2006). The study of the northern part of the Tan–Lu fault zone still remains controversial. The origin models of the northern extension of the Tan–Lu fault zone are either normal faulting models (Xu et al., 1984; Liu et al., 1993; Zhang et al., 2005), sinistral transtension models (Yin et al., 2005; Wang et al., 2012), or sinistral transpression models (Wang et al.,

* Corresponding author. E-mail: liuyongjiang@ouc.edu.cn

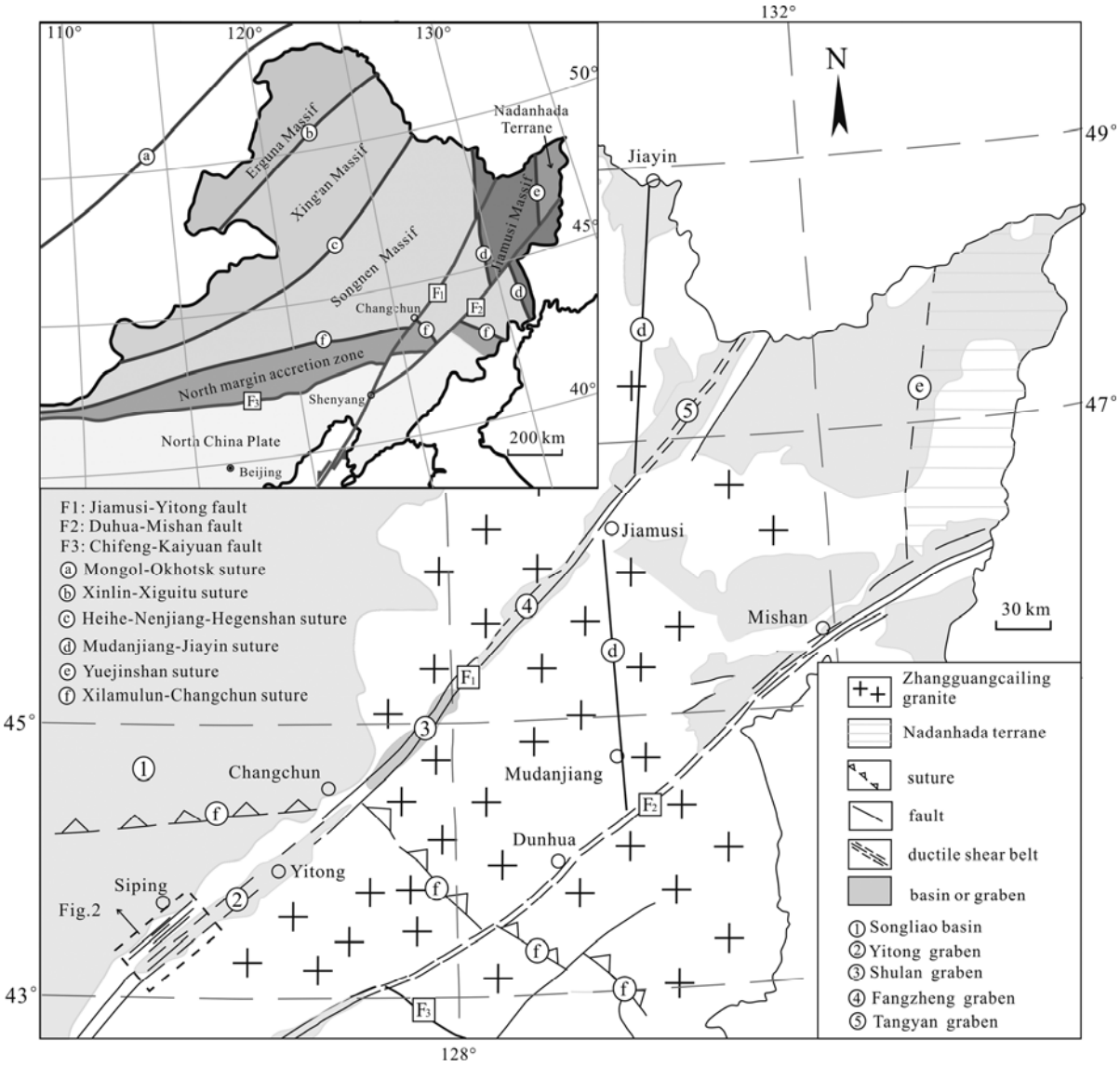

Fig. 1. Structural sketch for Jiamusi–Yitong Fault Zone and its surrounding area (modified from Sun et al., 2008; Zhou et al., 2009).

2000; Zhu et al., 2002, 2003, 2004, 2010; Liang et al., 2015). As a branch of the northern Tan–Lu fault zone, previous researchers have paid more attention to the formation time of the JYFZ, such as in the Triassic (Wan, 1995; Guo et al., 2000; Li et al., 2008), late Triassic to early Jurassic (Zhang and Dong, 2008), late Jurassic (Zhu et al., 2010), late Jurassic to early Cretaceous (Yin et al., 2005) or early Cretaceous periods (Xu et al., 1987; Chen, 1988; Dou et al., 1996; Wang et al., 2000; Zhu et al., 2002, 2003, 2004; Sun et al., 2006; Han et al., 2012; Meng et al., 2013; Liang et al., 2015; Gu et al., 2016； Sun et al., 2016). Based on previous studies, we present a detailed field investigation and laboratory analysis of the ductile structure of the origin of the JYFZ and determined the geometric and kinematic features. To solve the issues mentioned above, we sampled and measured muscovite from the mylonite in the JYFZ shear zone for $^{40}Ar/^{39}Ar$ dating and thus determined the strike–slip time. We also performed a dynamic background analysis of the origin of the JYFZ. Based on our study, we provide updated evidence to illustrate the history of the entire Tan–Lu Fault Zone evolution process to aid the understanding of the dynamic processes in NE China.

2 Geological Setting

The southern end of the JYFZ starts from Shenyang and passes through the North China Plate and successively to the north margin accretion zone of the North China Plate, Songnen Massif, and Jiamusi Massif in the northeast. It also cuts through the Chifeng–Kaiyuan fault, the Xilamulun–Changchun suture, and Mudanjiang suture successively from the south to the north (Fig. 1). The Neoarchean–Paleoproterozoic advanced metamorphic basement and middle Neoproterozoic marine covered strata are mainly exposed in the south of the JYFZ

(LBGMR, 1989). Late Paleozoic and Mesozoic–Cenozoic granites and Permian and Mesozoic–Cenozoic sedimentary rocks are primarily exposed in the central region (JBGMR, 1989). Paleozoic–Mesozoic granites, Paleozoic–Mesozoic volcanic–sedimentary rock series (HBGMR, 1993), Heilongjiang complex with blue schist facies (Zhou et al., 2009; Li et al., 2014), and the high-grade metamorphic Mashan group (Wu et al., 2007a, 2011; Zhou et al., 2009a; Wilde et al., 2003) are mainly exposed in the north.

Strong extensional activity occurred in the early Cretaceous in Northeast China, which was characterized by extensive magmatic activities and the development of fault basins (Wu, et al., 2002). Along the JYFZ, a series of grabens also developed in the early Cretaceous, including YitongShulan, Fangzheng, and Tangyan Grabens from south to north (Fig. 1). The strata in the Yitong and Shulan Garbens are divided from the bottom to the top into lower Cretaceous Yingchengzi, Denglouku, and Quantou formations and into Paleogene Shuangyang, Yongji, Wanchang, and Chaluhe formations (Liu et al., 1993). The strata in the Fangzheng and Tangyuan Grabens are divided into upper Cretaceous Houshigou and Dongshan formations, Paleogene Wuyun, Xin'ancun, Dadahe, and Baoquanling formations, and the Neogene Fujin and Chuandishan formations from bottom to top (Wan et al., 2014). The neogene eruption of mantle–derived basalts occurred locally along JYFZ, suggesting that the fault zone cut through the lithospheric mantle (Zhang et al., 2006; Zhou et al., 2010).

Thus far, considerable isotopic dating data has been reported for the middle to southern segment of the Tan–Lu fault zone (Zhu et al, 2001, 2004; Chen et al., 2000; Wang, 2006). However, there is no detailed isotopic dating for the JYFZ, which directly limits the determination of the age of the sinistral strike–slip activity of the JYFZ. To investigate further, we selected mylonites exposed to the west of the Yitong Graben in the JYFZ to perform zircon U–Pb dating, muscovite $^{40}Ar/^{39}Ar$ dating, and determined the microstructures. Our research results fill the gaps of the isotopic age of mylonite in the JYFZ and add new evidence to the determination of the sinistral strike–slip age of the northern section of the Tan–Lu fault zone.

3 Structures of the Strike–slip Ductile Shear Belts

The shear belt appears along the west of the Yitong Graben, and the mylonite samples were taken from the Zhangjia village in Shuangmiaozi town (Fig. 2). The shear belt has a total width of 1–1.5 km (Fig. 2). The original rock of the mylonite was granite, which was formed in the Permian. The mylonites are reddish in color with particle sizes of 0.1–1 mm. The shear belt showed widespread ductile deformation with dense foliations (Fig. 3a, 4b). The shear belt strike was at NE 45° preferentially and dipped NW at 75–80° (Fig. 3a, 4b). Many oriented samples were collected from the shear belt. Microscopic observation showed that most rocks in the shear belt are mylonitized rocks. S–C fabrics, rotated feldspars, and quartz porphyroclasts from the oriented thin sections indicated a sinistral shear sense (Fig. 3c–f).

3.1 Microstructures of the shear belts

Microstructures were well obtained in the shear belt. Quartz mainly acts as the matrix, which is characterized

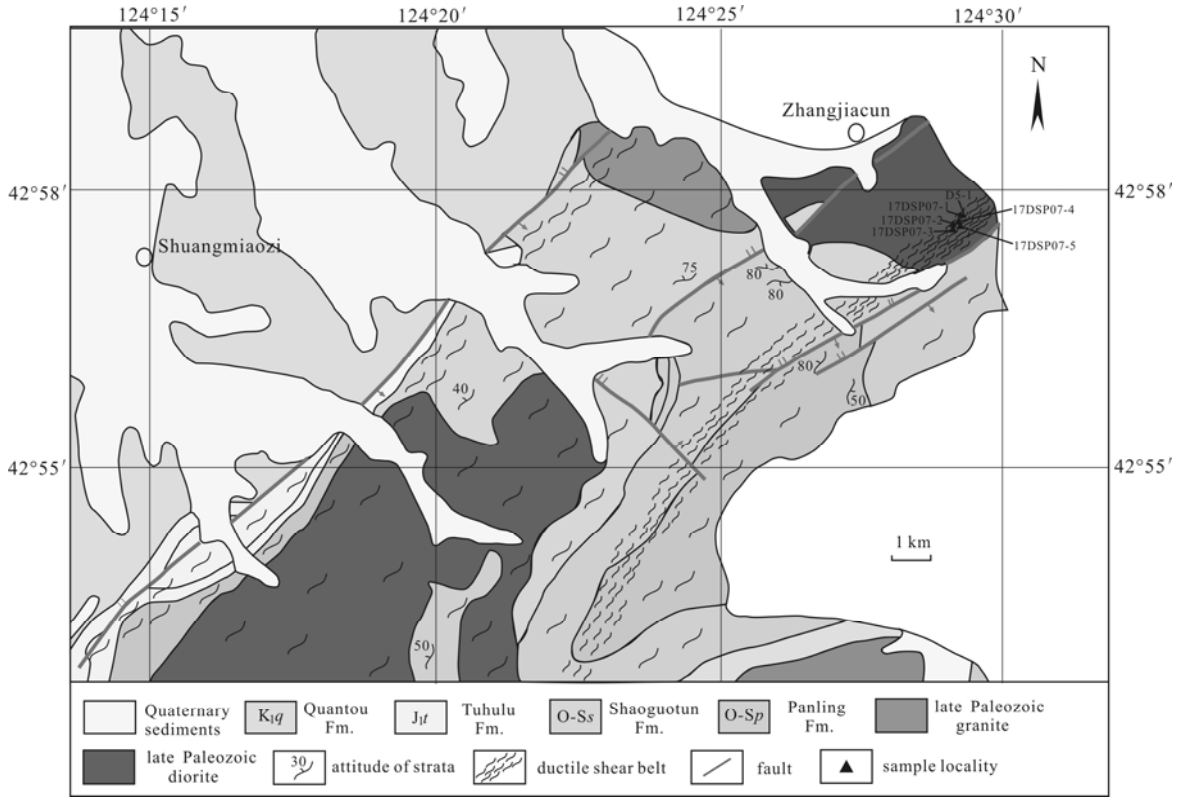

Fig. 2. Simplified geological map of the JYFZ shear belt showing the tectonic framework and the distribution of strata.

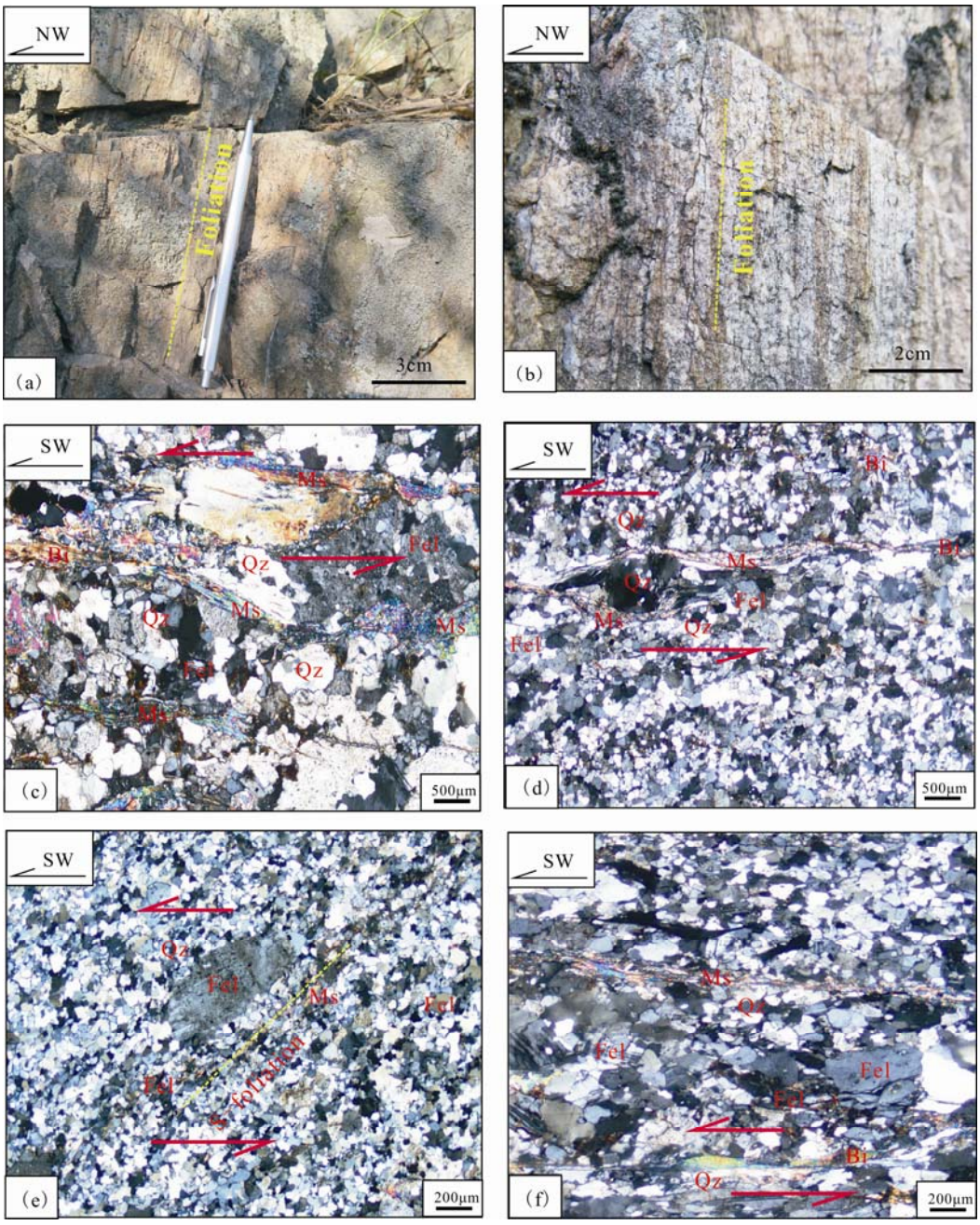

Fig. 3. Outcrop photographs and photomicrographs (crossed polarizers) for rocks of the JYFZ.
(a) Steep mylonite belt(17DSP07–2); (b) steep mylonite belt(17DSP07–3); (c) granitic mylonite (17DSP07–2), showing quartz dynamitic recrystallization of both subgrain rotation (SR) and grain boundary migration (GMB) as well as sinistral shear sense presented by S–C fabrics and rotated Quartz; (d) granitic mylonite (17DSP07–3), showing quartz SR recrystallization and sinistral shear sense indicated by S–C fabrics and rotated quartz; (e) granitic mylonite (17DSP07–4), presenting quartz SR recrystallization and sinistral shear sense indicated by rotated feldspar porphyroclast; (f) granitic mylonite (17DSP07–5), exhibiting quartz SR recrystallization and sinistral S–C fabriscs.

by plastic elongation and directional arrangement. Polycrystalline quartz and newborn muscovites often constitute C–foliation (Fig. 3c–f). Most quartz in the matrix showed dynamitic recrystallization of subgrain rotation (SR). Mineral deformation in the mylonites was closely related to the deformation temperatures and can, therefore, be used to estimate the deformation temperatures (Essene, 1989). Previous studies (Tullis and Yund, 1991; Stipp et al., 2002) demonstrated that quartz BLG, SR, and GBM recrystallization correspond to deformation temperatures of 300–400°C, 400–500°C, and >500° C, respectively. Brittle fracturing, flattening and elongation, and marginal subgrains in the feldspar suggested deformation temperatures of 300–400°C, 400–500°C, and >500°C respectively. The temperature of the symbiotic muscovite and biotite was generally above 440°C (Hoisch, 1989). Deformation behaviors of quartz and feldspar and the assemblage in the JYFZ (Table 1)

suggest that the deformation temperatures were approximately 450°–500°C or 450°–550°C locally, which was similar to that of the medium to high greenschist facies.

3.2 Quartz c–axis fabrics

To better understand the microstructures of the shear belt, four oriented mylonite samples were chosen for quartz *c*–axis fabric analysis. The analysis was conducted using electron backscatter diffraction in the Key Laboratory of Mineral Resources Evaluation in Northeast Asia, Ministry of Land and Resources, Jilin University, Changchun, China, and the analytical procedures and machine parameters have been previously described in Liu et al. (2008).

Quartz *c*–axis fabric plots of the four mylonites samples from the shear belts showed both predominately activity of the rhomb <a> and cylindrical <a> slip systems (Fig. 4). The activities of the different slip systems are related to the deformation temperatures (Passchier and Trouw, 2005). Therefore, it is suggested that the four mylonitic samples have medium to high-grade temperature deformation characteristics. The deformation temperature was 450–500° C. These estimated deformation temperatures are consistent with those estimated from mineral deformation behaviors (Table 1). The lines of central concentration of the four samples were inclined to the left relative to the central axis, which indicates a sinistral shear sense or top–to–NE sense of shear, which is consistent with the microscopic observations.

3.3 Finite strain type discrimination

This study was based on the measurement principle of the Fry method (Fry, 1979; Zheng, 1985). Two oriented thin sections from the XZ and YZ planes were prepared, and micrographs were taken from the regions where the particles were evenly distributed under the microscope. In CorelDRAW 17, to calibrate the micrograph of the quartz residual spot center, we selected the image center as the origin and removed the point of origin to a particular spot center according to traditional calibration methods and the rest of the silica residue at the center of the reciprocating calibration to cover the entire spot center. The blank area in the center of the image after translation of the center of the quartz speckle represented the strain ellipse, and its length and length axes were measured. Specific measurement data are shown in Table 2. A Flinn diagram was used to distinguish the finite strain measurement results for the deformed rocks in the ductile shear zone of the JYFZ.

Based on the discrimination of finite strain types using the Flinn diagram, the finite strain types for the deformed mylonite were uniform with a K‐value (K=ln (X/Y) /ln (Y/Z)) that was significantly less than 0.5 (Table 2 and Fig. 5) and characterized by compressional strain.

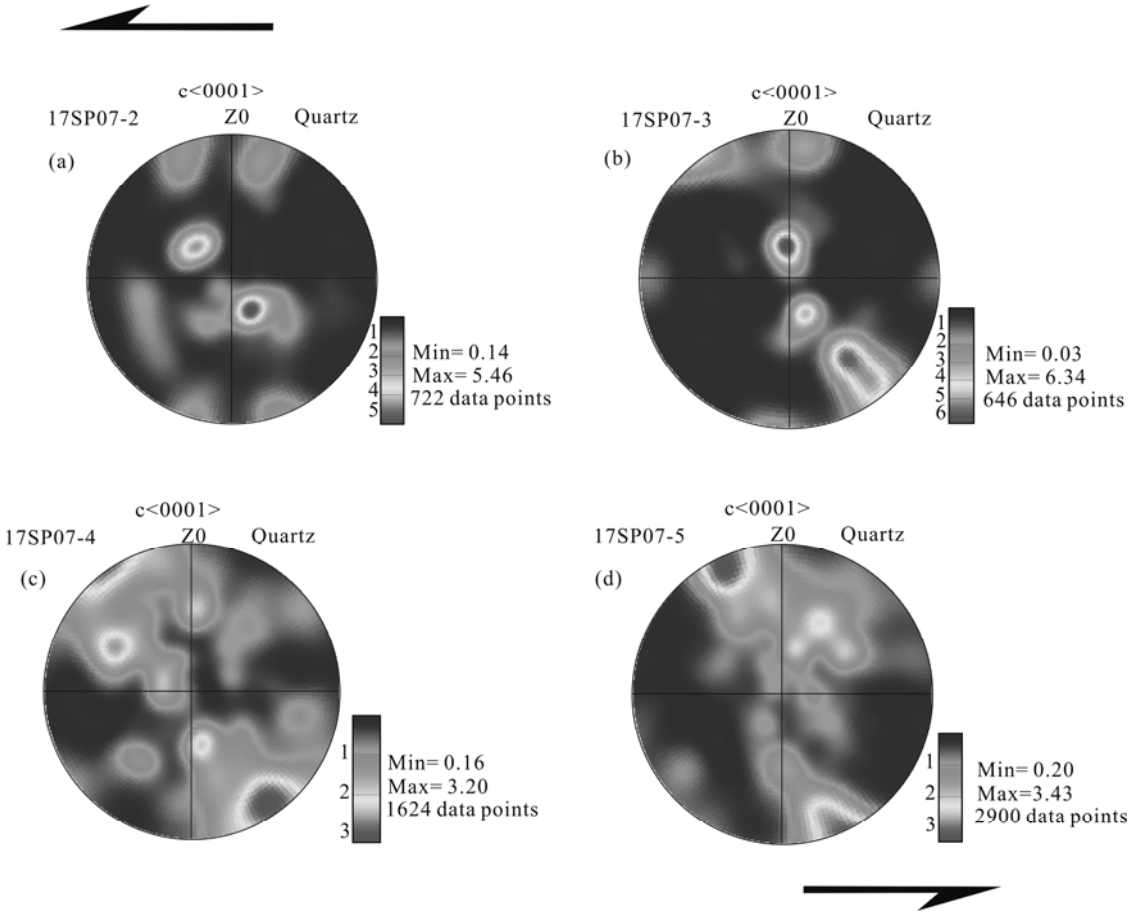

Fig. 4. Quartz *c*–axis fabric plots for samples from the shear belt.

Table 1 Microstructures of mylonite samples from the JYFZ shear zones and P–T estimates [a)]

Sample No.	Rock type	Locality	Assemblage	Feldspar deformation	Quartz deformation	Estimated *T* (°C)
17DSP07–2	Mylonite	N: 42°57′57.03″; E: 124°28′52.05″	Fel+Qz+Bi+Ms	Elongated	SR	450°–500℃
17DSP07–3	Mylonite	N: 42°57′57.04″ E: 124°28′52.07″	Fel+Qz+Bi+Ms	Elongated	SR+GMB	450°–550℃
17DSP07–4	Mylonite	N: 42°57′57.03″ E: 124°28′53.02″	Fel+Qz+Bi+Ms	Elongated	SR	450°–500℃
17DSP07–5	Mylonite	N: 42°57′57.02″ E: 124°28′52.02″	Fel+Qz+Bi+Ms	Elongated	SR	450°–500℃

a) Qz–quartz; Fel–feldspar; Bi–biotite; Ms–muscovite; SR–subgrain rotation crystallization; GBM–grain boundary migration crystallization

4 Zircon U–Pb Dating for Plutons in the Shear Belts

4.1 Analytical methods

To determine the age of the original rocks in the ductile shear zone, zircon U–Pb dating of 17DSP7–1 (GPS: 42° 57' 57.03″N; 124°28' 52.05″E) was performed (Fig. 2). Single mineral separation of zircon was completed by a Yuneng Mineral Separation Service Company in Langfang, Hebei Province. The sample was crushed using conventional methods and separated by flotation, electromagnetic separation, and other methods and then manually selected using binoculars. The separated zircon grains were fixed with epoxy resin and polished until the zircon was exposed to the core. The sample surface was cleaned and decontaminated using HNO_3 solution at a volume percentage of 3%. The transmitted light, reflected light, and cathodoluminescence (CL) image were completed by the Beijing Zhongke Rock Mine Detection Technology Company. The LA–ICP–MS U–Pb zircon dating was performed at the Key Laboratory of Mineral Resources Evaluation in Northeast Asia, Ministry of Land and Resources, Jilin University, Changchun, China. CL imaging involves mono CL3 + cathode luminescence produced by Gatan, Inc. (UK). The zircon dating work included ICP–MS using the latest generation Agilient 7500a (with Shield Torch). The laser denuding system was the GeoLas200M, which was produced by the MicroLas Company (Germany). The laser denudation was performed using one time denudation with helium as the carrier gas for the denudation material. The diameter of the laser beam was 32 μm, the frequency was 10 Hz, and the laser energy was 90 mJ. The gas background acquisition time for each analysis point was 20 s, and the signal acquisition time was 40 s. The specific testing procedures and lead correction methods have been described by Yuan et al., 2008, Diwu et al., 2008, and Andersen, 2002.

4.2 Isotope dating of the zircons

CL images of the representative zircon grains are shown in Fig. 6a, and the LA–ICP–MS zircon U–Pb data are presented in Table 3. The zircon grains from granite are typically euhedral to subhedral, with lengths of 80–150 μm and length–to–width ratios of 1:1 to 2:1. The zircons displayed oscillatory zoning in the CL images and some contained opaque inclusions (Fig. 6a). The zircon Th/U values ranged from 0.43 to 1.37 (Table 3), suggesting that the calculated zircon was of magmatic origin. In the $^{207}Pb/^{235}U$–$^{206}Pb/^{238}U$ concordia diagrams (Fig. 6b), all the plots are along the concordia line with a narrow age range. The sample yield weighted mean of the U–Pb zircon ages was 264.1.1±1.1 Ma. The age indicates that the granite emplaced during the middle Permian.

Table 2 Finite strain results from the selected Mylonite of the shear belts

Sample no.	$R_{S-X/Z}$	$R_{S-Y/Z}$	$R_{S-X/Y}$	k
17DSP07–2	1.8	1.58	1.14	0.28
17DSP07–3	1.5	1.4	1.07	0.21
17DSP07–4	1.71	1.54	1.11	0.24
17DSP07–5	1.67	1.42	1.18	0.46

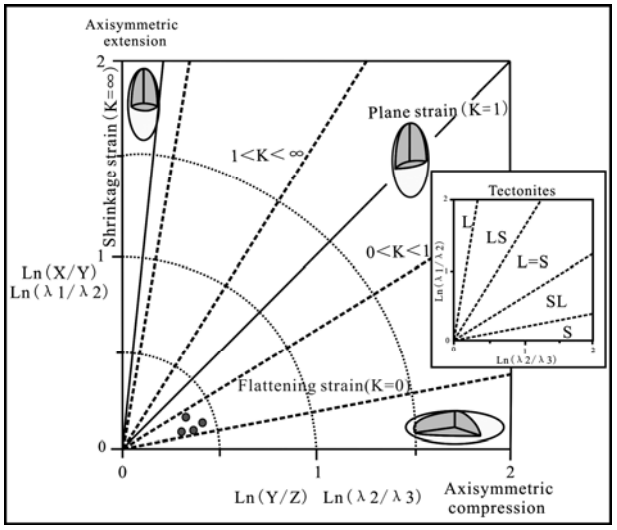

Fig. 5. Flinn finite strain discrimination diagram from the selected mylonite of the shear belts.

5 Muscovite $^{40}Ar/^{39}Ar$ Dating from Mylonite in the Shear Belts

5.1 Analytical methods

To determine the sinistral strike–slip shear age of JYFZ, muscovite $^{40}Ar/^{36}Ar$ dating of D5–1 (GPS: 42°57'57.03″ N; 124°28'52.05″E) was conducted (Fig. 2). The rock sample was crushed manually using an iron mortar, and the powder of the rock was separated through a sieve for different particle sizes. The primary muscovites were artificially purified under binoculars after repeated flotation with water. The selected muscovites were placed in the B8 channel of a 49–2 reactor for neutron irradiation at the Chinese Institute of Atomic Energy and then completed using the full-time standard, fully automatic, high-precision, and high-sensitivity $^{40}Ar/^{39}Ar$ dating laser

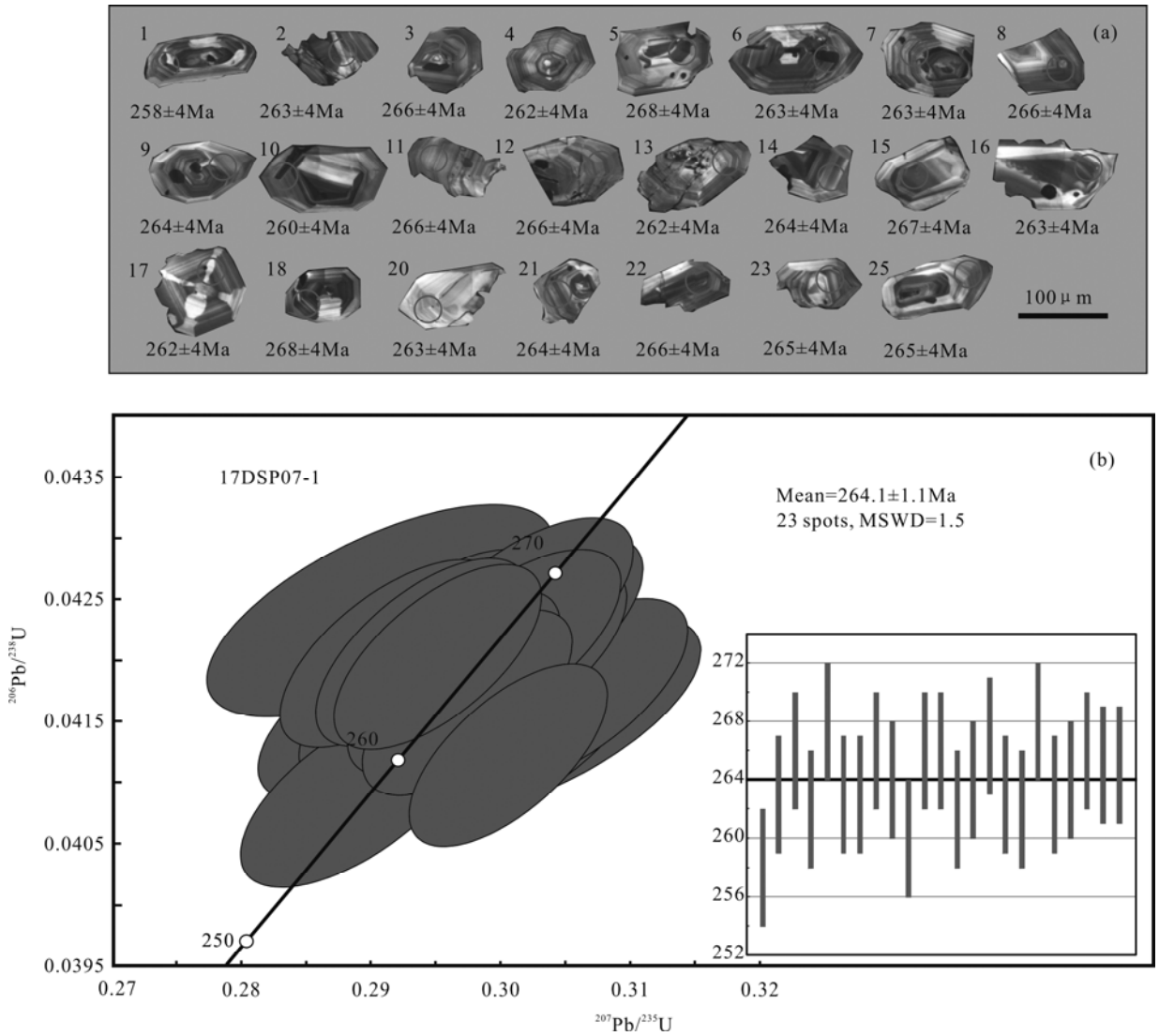

Fig. 6. Cathodoluminescence (CL) images and zircon U–Pb concordia diagrams from 17DSP07–1 sample.
(a) Circles indicate the location and size of dating spots. The numbers below the zircons refer to the U–Pb ages, and those above the zircons refer to the numbers of dating; (b) Zircon U–Pb concordia diagrams for granite in the shear belts

system in the Key Laboratory of Orogenic Belt and Crustal Evolution, Ministry of Education, Peking University. The irradiation time was 24 h, and the fast neutron flux was 5.184×10^{19}. The standard sample used for neutron flux monitoring came from biotite of granite ZBH–25 from Zhoukoudian, Beijing, and the age of the standard sample was 132.7 Ma (Sang, 2006). The standard reference for muscovite is BERN–4M in Germany, which has good uniformity and an age of 18.6 Ma (Purdy and Jäger, 1976). At the same time, pure CaF_2 and K_2SO_4 were simultaneously irradiated to obtain the correction factor. The single muscovite was melted by focusing the laser. The system testing process, raw data processing, model age, and isochron age calculations were all automatically controlled by MASS SPEC (v.5.02) software written by Alan L. Denio at the Center for Geochronology, University of California, Berkeley. More detailed analytical conditions and procedures can be found in Lo et al. (2002) and Lee et al. (2003).

5.2 Isotope dating of muscovite

The dating results are shown in Table 4. The isochron age of $^{40}Ar/^{36}Ar$–$^{39}Ar/^{36}Ar$ was 162.7±1.0 Ma (Fig. 7a). The initial value for $^{40}Ar/^{36}Ar$ was 300 ± 18, and if the error was taken into account, it was in the same range as the current atmospheric $^{40}Ar/^{36}Ar$ value. The data points for 21 muscovites obviously showed a linear relationship. In addition, the obtained 21 ages were very similar and were concentrated at 161–165 Ma with a peak age of 162.8±1.2 Ma (Fig. 7b), which is highly consistent with the isochronological age. Therefore, the ages of the $^{40}Ar/^{36}Ar$–$^{39}Ar/^{36}Ar$ isochrones obtained in this study are believed to be reliable and applicable to geological interpretation. Zhu et al. (2004, 2005) measured a large number of mica $^{40}Ar/^{39}Ar$ isotopic ages in the middle and southern section of the Tan–Lu fault zone, including both plateau ages and isochronic ages. The error between the isotopic plateau ages and isochronic ages in the same sample that can be used for geological interpretation is no

Table 3 LA-ICP-MS U-Th-Pb isotopic data of zircon in the sample 17DSP07–1

Spot no.	Th/U	Isotopic ratio						Ages (Ma)						Concordance analysis
		$^{207}Pb/^{206}Pb$	1σ	$^{207}Pb/^{235}U$	1σ	$^{206}Pb/^{238}U$	1σ	$^{207}Pb/^{206}Pb$	1σ	$^{207}Pb/^{235}U$	1σ	$^{206}Pb/^{238}U$	1σ	
1	0.78	0.05121	0.00150	0.28885	0.00733	0.04090	0.00062	250	32	258	6	258	4	100%
2	0.45	0.05303	0.00153	0.30510	0.00757	0.04172	0.00064	330	30	270	6	263	4	102.7
3	0.63	0.05073	0.00146	0.29470	0.00729	0.04212	0.00064	229	30	262	6	266	4	98.5
4	0.90	0.05276	0.00160	0.30121	0.00795	0.04140	0.00064	318	33	267	6	262	4	101.9
5	1.17	0.04970	0.00203	0.29061	0.01090	0.04240	0.00071	181	56	259	9	268	4	96.6
6	0.95	0.05178	0.00137	0.29739	0.00661	0.04165	0.00062	276	26	264	5	263	4	100.4
7	0.67	0.05220	0.00166	0.29933	0.00837	0.04158	0.00065	294	36	266	7	263	4	101.1
8	0.74	0.05026	0.00141	0.29144	0.00699	0.04205	0.00063	207	29	260	5	266	4	97.7
9	0.91	0.05123	0.00167	0.29482	0.00853	0.04173	0.00065	251	39	262	7	264	4	99.2
10	1.24	0.05287	0.00133	0.30050	0.00625	0.04122	0.00061	323	23	267	5	260	4	102.7
11	0.57	0.05138	0.00188	0.29809	0.00985	0.04207	0.00068	258	47	265	8	266	4	99.6
12	0.68	0.05172	0.00144	0.30047	0.00713	0.04213	0.00063	273	29	267	6	266	4	100.4
13	0.66	0.05148	0.00155	0.29415	0.00768	0.04143	0.00063	262	33	262	6	262	4	100
14	1.14	0.05139	0.00138	0.29633	0.00670	0.04181	0.00062	258	27	264	5	264	4	100
15	0.50	0.05181	0.00150	0.30169	0.00753	0.04223	0.00064	277	31	268	6	267	4	100.4
16	0.43	0.05090	0.00175	0.29227	0.00902	0.04164	0.00066	236	42	260	7	263	4	99.8
17	0.76	0.05286	0.00198	0.30279	0.01028	0.04153	0.00068	323	48	269	8	262	4	100.7
18	1.37	0.05155	0.00145	0.30130	0.00726	0.04238	0.00064	266	29	267	6	268	4	99.6
20	0.58	0.05207	0.00195	0.29934	0.01017	0.04169	0.00068	288	48	266	8	263	4	101.1
21	0.80	0.05213	0.00157	0.30038	0.00786	0.04179	0.00064	291	33	267	6	264	4	101.1
22	0.79	0.05066	0.00137	0.29385	0.00668	0.04206	0.00063	225	27	262	5	266	4	98.9
23	0.69	0.05189	0.00148	0.30064	0.00736	0.04201	0.00063	281	30	267	6	265	4	100.8
25	0.56	0.05092	0.00134	0.29507	0.00652	0.04202	0.00062	237	26	263	5	265	4	99.2

Table 4 $^{40}Ar/^{39}Ar$ analytical data of muscovite from the sample D5–1

Run ID	Sample	%40*	Age(Ma)	±	36/39	±36/39	37/39	±37/39	38/39	± 38/39	40/39	± 40/39	40*/39	±40*/39
20338–01	D5–1	95.04	164	1	0.00353	0.00012	0.000	0.002	0.0127	0.0002	21.02	0.05	19.97	0.06
20338–02	D5–1	95.08	163	1	0.00348	0.00013	0.001	0.002	0.0127	0.0002	20.90	0.09	19.87	0.10
20338–03	D5–1	95.93	163	1	0.00286	0.00013	0.010	0.002	0.0128	0.0002	20.77	0.05	19.92	0.07
20338–04	D5–1	95.14	164	1	0.00346	0.00007	0.003	0.001	0.0127	0.0001	21.05	0.06	20.02	0.06
20338–05	D5–1	94.99	163	1	0.00354	0.00008	0.006	0.002	0.0126	0.0001	20.89	0.05	19.84	0.05
20338–06	D5–1	94.05	163	1	0.00427	0.00009	0.003	0.002	0.0130	0.0001	21.21	0.05	19.94	0.06
20338–08	D5–1	95.48	161	1	0.00316	0.00007	0.002	0.001	0.0127	0.0001	20.64	0.05	19.71	0.06
20338–09	D5–1	95.90	163	1	0.00289	0.00008	0.004	0.002	0.0127	0.0001	20.81	0.05	19.95	0.05
20338–10	D5–1	94.36	164	1	0.00406	0.00015	0.004	0.003	0.0129	0.0002	21.28	0.05	20.07	0.07
20338–11	D5–1	94.09	162	1	0.00421	0.00012	0.009	0.002	0.0133	0.0002	21.04	0.05	19.79	0.06
20338–12	D5–1	96.31	162	1	0.00256	0.00010	0.003	0.002	0.0128	0.0002	20.49	0.04	19.73	0.05
20338–13	D5–1	95.65	161	1	0.00302	0.00024	0.008	0.004	0.0117	0.0003	20.53	0.04	19.64	0.09
20338–14	D5–1	94.72	162	1	0.00375	0.00011	0.005	0.002	0.0126	0.0001	20.94	0.05	19.83	0.06
20338–15	D5–1	95.55	165	1	0.00321	0.00034	0.008	0.005	0.0120	0.0004	21.34	0.05	20.39	0.12
20338–16	D5–1	87.34	162	1	0.00973	0.00017	0.003	0.003	0.0137	0.0003	22.71	0.06	19.83	0.08
20338–17	D5–1	90.59	163	1	0.00699	0.00013	0.005	0.002	0.0136	0.0002	21.96	0.04	19.89	0.06
20338–19	D5–1	89.02	164	1	0.00838	0.00016	0.004	0.002	0.0134	0.0002	22.56	0.05	20.08	0.07
20338–20	D5–1	96.34	164	1	0.00259	0.00015	0.042	0.003	0.0127	0.0002	20.79	0.06	20.03	0.07
20338–21	D5–1	95.86	163	1	0.00291	0.00016	0.009	0.003	0.0128	0.0002	20.74	0.05	19.88	0.07
20338–23	D5–1	92.92	161	1	0.00507	0.00020	0.011	0.003	0.0133	0.0002	21.16	0.07	19.65	0.09
20338–24	D5–1	93.56	161	1	0.00458	0.00014	0.007	0.003	0.0130	0.0002	21.00	0.07	19.64	0.08

J=0.00474; ±J=4.85E–05

more than 2%, and the two age are highly consistent. Therefore, we believe that the isochronal ages can also accurately reflect the ages of tectonic thermal events. The granite in the shear belts was formed at ~264 Ma. Because the shear zone's deformation temperature (approximately 450–500° C) was higher than the muscovite closure temperature (300–400° C) (Ehlers et al., 2005), the muscovite laser $^{40}Ar/^{39}Ar$ age (162.7±1.0 Ma) represents the time of the sinistral shear strike of the JYFZ.

6 Discussion

In recent years, significant achievements have been made on properties and evolutionary stages of the Tancheng–Lushan fault zone in Eastern China (Chen et al., 2000; Zhu et al., 2001, 2005; Wang et al., 2006; Zhang, et al., 2008; Zhang and Dong, 2008). According to the preliminary analysis of the geochronological data, at least three stages of strike–slip events occurred in the Tan–Lu fault zone: (1) at 236–238 Ma during the middle Triassic, which is the deep subduction stage of the collision between the North China Plate and the south China Plate, which likely originated from the intracontinental transition fault and lasted to the end of the Triassic (Zhang et al., 2008; Chen et al., 2000); (2) in the middle Jurassic to the late Jurassic (155–165 Ma), which was the sinistral compression strike–slip period (Wang et al., 2006; Sun et al., 2008; Han, et al., 2014); and (3) at 137–143 Ma in the early Cretaceous, which was the sinistral strike–slip shear period (Zhu et al., 2001, 2005).

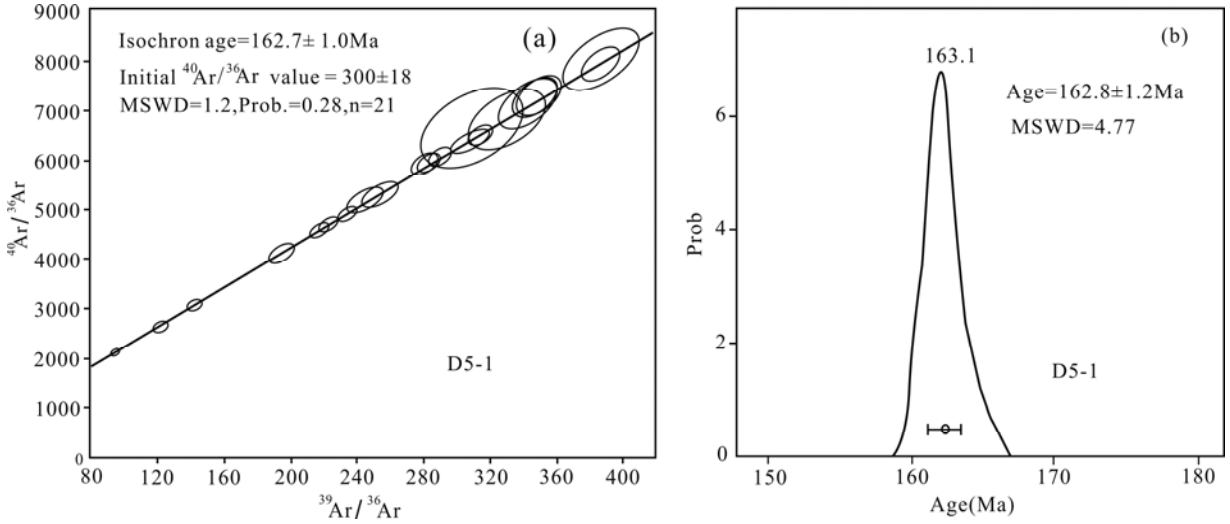

Fig. 7. $^{40}Ar/^{39}Ar$– $^{40}Ar/^{36}Ar$ isochron age and peak age of muscovite in mylonite

In northeastern China, the strike–slip ages for the JYFZ and Dunhua–Mishan fault zone mainly include the following. Sun et al. (2008) obtained a muscovite $^{40}Ar/^{39}Ar$ isochron age of 164±2 Ma for a sample collected in the mylonite of the ductile shear zones in the Dunhua–Mishan fault zone and indicated a second sinistral strike–slip shear event about the Tan–Lu fault zone. Dou et al. (1996) conducted $^{40}Ar/^{39}Ar$ single mineral analysis of mica quartz schist and diabase from the JYFZ and obtained plateau ages of 100 ± 2.3 Ma and 105 Ma, which may reflect the late extension event of JYFZ. Yin et al. (2005) determined the biotite $^{40}Ar/^{39}Ar$ plateau age of 133.13±0.31 Ma for crushed fine-grain biotite monzonitic granite and the muscovite $^{40}Ar/^{39}Ar$ plateau age of 135.66±0.11 Ma, which corresponds to the third sinistral strike–slip shear event. In this study, our new muscovite $^{40}Ar/^{39}Ar$ isochron age was determined to be 162.7±1 Ma, which is consistent with the strike–slip times of the second domain of the Tan–Lu fault zone and the Dunhua–Mishan fault zone.

Considering the dynamic background, during ~180 Ma, the Farallon Plate subducted northwestward beneath the Eurasian Plate at a speed of 10.7 cm/y; thus, a drag effect on the eastern margin of the Eurasia northeastwards undoubtedly occurred. The ~150 Ma Izanazi Plate subducted northward beneath the Eurasian continent at a high speed (30 cm/y), which produced NW compression on the Eurasian continent and a large NE strike–slip component along the continental NE margin (Maruyama et al., 1997). Combined with the previously reported ages of the Tan–Lu fault zone, the NE strike–slip faults and the Heilongjiang group of blueschist rapidly underwent subduction exhumation, and during ~160 Ma, NE strike–slip shear events occurred in northeastern and even in East China. Owing to the changing of the subduction angle of the west Pacific Plate (including the Farallon and Izanazi Plates) subducting beneath the Eurasian continent, many strike–slips occurred, which were related to the strike–slip adjustment during terrane collisions (Zhao et al., 1994; Maruyama et al., 1997).

7 Conclusion

From both structural and geochronological studies along the JYFZ, the following main conclusions can be made:

(1) The exposed ductile shear belts strike northeastward with steep foliations. Outcrop structures, microstructures, and quartz *c*–axis fabrics all show a sinistral shear sense with minor reverse components for the shear belts.

(2) Microscopic observation and quartz *c*–axis fabrics suggest that the deformation temperature was approximately 450–500°C. Zircon U–Pb dating for granite was at 264.1±1 Ma, and the $^{40}Ar/^{39}Ar$ isochron age of muscovite was at 162.7±1 Ma for the JYFZ, which shows the age of the sinistral strike–slip shear of JYFZ. This is consistent with the second sinistral strike–slip shear event around the Tan–Lu fault zone.

(3) The late Jurassic initiation of the JYFZ was related to the speed and direction of oblique subduction of the West Pacific Plate under the Eurasian continent and to responsive terrane collision during the Jurassic period.

Acknowledgements

We thank Dr. Y.J. Hao from Key laboratory of Mineral Resources Evaluation in Northeast Asia, Ministry of Land and Resources, for his help on analysis of the zircon LA–ICP–MS U–Pb ages. This study was funded by the National Key R&D Program of China (Grant No. 2017YFC0601300–01), 973 Program (Grant 2013CB429802), NSFC (Grant 41102140，41303175).

Manuscript received May 15, 2019
accepted Aug. 24, 2019
associate EIC XIAO Wenjiao
edited by FEI Hongcai

References

Andersen, T., 2002. Correction of common lead in U–Pb analyses that do not report ^{204}Pb. Chemical Geology, 192(1–2): 59–79.

Chen, X.H., Wang, X.F., Zhang, Q., Chen, B.L., Chen, Z.L., Harrison, T.M., and Yin, A, 2000. Geochronologic study of the formation and evolution of the Tan–Lu fault zone. Journal of Jilin University (Earth Science Edition), 30(3): 215–220 (in Chinese with English abstract).

Chen. P.J., 1988. Timing and framework of huge displacement of the Tan–Lu Fault. Chinese Science Bulletin, 33: 289–293 (in Chinese).

Diwu, C.R., Sun, Y., Yuan, H.L., Wang, H.L., Zhong, X.P., and Liu, X.M., 2008. U–Pb ages and Hf isotopes for detrital zircons from quartzite in the Paleoproterozoic Songshan Group on the southwestern margin of the North China Craton. Chinese Science Bulletin, 53(18): 2828–2839.

Dou, L.R., Song, J.G., and Wang, Y., 1996. Chronology of the formation of the northern Tan–Lu fault zone and its implications. Geological Review, 42(6): 508–513 (in Chinese with English abstract).

Ehlers T.A., Chaudhri, T., Kumar, S., Fuller, C.W., Willett, S.D., Ketcham, R.A., Brandon, M.T., Belton, D.X., Kohn, B.P., Gleadow A.J.W., Dunai, T.J., and Fu, F.Q., 2005. Computation tools for low–temperature thermochronometer interpretation. Reviews in Mineralogy and Geochemistry, 58(1): 589–622.

Essene, E.J., 1989. The current status of thermobarometry in metamorphic rocks. In: Daly, J.S., Cliff, R.A., and Yardley, B.W. (eds), Evolution of Metamorphic belts. Geologica Society of Special Publication, 43: 1–44.

Fry, N., 1979. Random point distributions and strain measurements in rocks. Tectonophysics, 6: 89–105.

Gu, C.C., Zhu, G., Zhai. M.J., Lin, S.Z., Song, L.H., and Liu, B., 2016. Features and origin time of Mesozoic strike–slip structures in the Yilan–Yitong Fault Zone. Science in China Series D: Earth Sciences, 59: 2389–2410

Guo, M.X., Sun, W., Yin, G.Y., and Peng, Y.J., 2000. North–extension of the Tanlu fracture and geologic–geophysical characteristics. Jilin Geology, 19: 35–44 (in Chinese with English with abstract).

Han, G.Q., Liu, Y.J., Neubauer, F., Gohann, G., Zhou, Y.X., Li, W., and Liang, C.Y., 2012. Characteristics, timing, and offsets of the middle–southern segment of the western boundary strike–slip fault of the Songliao Basin in Northeast China. Science in China Series D: Earth Sciences, 55: 464–475.

Han, G.Q., Liu, Y.J., Neubauer, F., Genser, J., Liang, C.Y., Wen, Q.B., and Zhao, Y.L., 2014. Chronology of L–Type tectonite from Nierji area in the northern–middle segment of the western boundary fault of the Songliao Basin and its tectonic implications. Acta Petrologica Sinica, 30(7): 1922–1934 (in Chinese with English abstract).

HBGMR (Heilongjiang Bureau of Geology and Mineral Resources), 1993. Regional geology of Heilongjiang Province. Beijing: Geological Publishing House, 1–734 (in Chinese).

Hoisch, T., 1989. A muscovite – biotite geothermometer. American Mineralogist, 74: 565–572.

JBGMR (Jilin Bureau of Geology and Mineral Resources), 1989. Regional geology of Jilin Province. Beijing: Geological Publishing House, 1–698 (in Chinese).

LBGMR (Liaoning Bureau of Geological and Mineral Resources), 1989. Regional Geology of Liaoning Province. Beijing: Geological Publishing House, 1–855 (in Chinese).

Lee, H.Y., Chung, S.L., Wang, J.R., Wen, D.J., Lo, C.H., Yang, T.F., Zhang, Y., Xie, Y., Lee, T.Y., Wu, G., and Ji. J., 2003. Miocene Jiali faulting and its implication for Tibetan tectonic evolution. Earth and Planetary Science Letters, 205: 185–194.

Li, W.M., Liu, Y.J., Takasu, A., Zhao, Y.L., Wen, Q.B., Guo, X.Z., and Zhang, L., 2014. Pressure (P) –temperature (T) – time (t) paths of the blueschists from the Yilan area, Heilongjiang Province. Acta Petrologica Sinica, 30(10): 3085–3099 (in Chinese with English with abstract)..

Li, D.T., Hu, J.W., Li, J.H., Sun, P.H., Wang, X.O., and Liu, Z.Y., 2008. The Triassic left–lateral ductile shear zone of Tan–Lu Fault Zone and its deformation in Northern Liaoning Province. Geology and Resources, 17: 254–258 (in Chinese with English with abstract).

Liang, C.Y., Liu, Y.J., Meng, J.Y., Wen, Q.B., Li, W.M., Zhao, Y.L., Mi, X.N., and Zhang, L., 2015. Strain and fractal analysis of dynamically recrystallized quartz grains and rheological parameter estimation of Shulan Ductile Shear Zone. Earth Science, 40: 115–129 (in Chinese with English abstract).

Liu, J.L., Cao S.Y., Zou, Y.X., and Song, Z.J, 2008. EBSD analysis of rock fabrics and its application. Geological Bulletin of China, 27(10): 1638–1645 (in Chinese with English abstract).

Liu, M.Q., Yang, B.Z., Deng, J.G., and Zhou, Y.H., 1993. Geological tectonic features and evolution of Yitong–Shulan graben. Beijing: Geological Publishing House, 1–106 (in Chinese).

Lo, C.H., Chung, A.L., Lee, T.Y., and Wu, G., 2002. Age of Emeishan flood magmatism and relation to Permian–Triassic boundary events. Earth Planetary Science Letters, 198: 449–458.

Maruyama, S., Isozaki, Y., Kimura, G., and Terabayash, M., 1997. Paleogeographic maps of the Japanese Islands: Plate tectonic synthesis from 750 Ma to the present. Island Arc, 6 (1): 121–142.

Meng, J.Y., Liu, Y.J., Liang, C.Y., Wen, Q.B., Han, G.Q., Mi, X.N., and Zhang, Li., 2013. Characteristics of ductile deformation of Jiamusi–Yitong fault. Global Geology, 32: 800 –807 (in Chinese with English with abstract).

Purdy, J.W., and Jäger, E., 1976. K–Ar ages on rock–forming minerals from the Central Alps. Memoria of the Institute of Geology and Mineralogy, University of Padova, 30: 31–42.

Sang, H.Q., Wang, F., He, H.Y., Wang, Y.L., Y, L.K., and Zhu, R.X., 2006. Intercalibration of ZBH–25 biotite reference material untilized for K–Ar and $^{40}Ar/^{39}Ar$ age determination. Acta Petrologica Sinica, 32(12): 3059–3078 (in Chinese with English abstract).

Stipp, M., Stünitz, H., Heilbronner, R., and Schmid, S.M., 2002. The eastern Tonale fault zone: A "natural laboratory" for crystal plastic deformation of quartz over a temperature range from 250 to 700°C. Journal of Structural Geology, 4: 1861–1884.

Sun, X.M., Zhang, X.Q., He. S., Wang, P.J., Zheng, H., Wan, K., and Li, D.Z., 2016. Two important Cretaceous deformation events of the Dunhua–Mishan Fault Zone, NE China. Acta Petrologica Sinica, 32(4): 1114–1128 (in Chinese with English abstract).

Sun, X.M., Liu, Y.J., Sun, Q.C., Han, G.H., Wang, S.Q., and Wang, Y.D., 2008. $^{40}Ar/^{39}Ar$ Geochronology evidence of strike–slip movement in Dunhua–Mishan fault zone. Journal of Jilin University (Earth Science Edition), 38(6): 965–972 (in Chinese with English abstract).

Sun, X.M., Long, S.X., Zhang, M.S., Liu, X.Y., and Hao, F.J., 2006. Discovery and timing of major thrust belt in Jiamusi–Yitong fault zone. Oil and Gas Geology, 27: 637–643(in Chinese with English abstract).

Tullis, J., and Yund, R.A., 1991. Diffusion creep in feldspar aggregates: Experimental evidence. Journal of Structural Geology, 13: 987–1000.

Wan, C.B., Xue, Y.F., Jin, Y.D., Zhang, X., and Zhang, S.X., 2014. New progresses of Mesozoic and Cenozoic s tratigraphic division and correlation study for Yishu graben. Petroleum Geology and Oilfield Development in Daqing, 33 (5): 179–185 (in Chinese with English abstract).

Wan, T.F., Zhu, H., Zhao, L., Lin, J.P., Cheng, J., and Chen, J., 1996. Formation and evolution of Tancheng–Lujiang Fault Zone: A review. Earth science, 10: 159–168 (in Chinese with English with abstract).

Wang, S.Q., Sun, X.M., Du, J.Y., Wang, Y.D., Xu, Q.W., Tian, J.X. 2012. Analysis of structural styles in northern segment of Tancheng–Lujiang Fault Zone. Geology Review, 58: 414–425 (in Chinese with English abstract).

Wang, X.F., Li, Z.J., Chen, B.L., Chen, X.H., Dong, S.W., Zhang, Q., Wu, H.L., Xing, L.S., Zhang, H., Dong, F.X., Wu, H.M., Huo, G.H., Lin, C.Y., Bai, J.Q., and Liu, X.C., 2000. Tan–Lu Fault Zone. Beijing: Geological Publishing House, 1–362 (in Chinese with English with abstract).

Wang, X.S., Zheng, Y.D., Liu, Y.L., Bradley, R., and Scott, F., 2006. The formation age of the chloritized zone in the Louzidian extensional detachment fault south of Chifeng,

Inner Mongolia, China. Progress in Natural Science, 16(7): 902–906 (in Chinese with English abstract).
Wang, Y., 2006. The onset of the Tanlu fault movement in eastern China: Constraints from zircon (SHRIMP) and $^{40}Ar/^{39}Ar$ dating. Terra Nova, 18: 423–431.
Wang, Y., and Dou, L.R., 1997. Formation time and dynamic characteristics of the northern part of the TanLu fault zone in east China. Seismology and Geology, 19(2): 186–194.
Wilde, S.A, Wu, F.Y, Zhang, X.Z., 2003. Late Pan–African magmatism in northeastern China: SHRIMP U–Pb zircon evidence from granitoids in the Jiamusi Massif. *Precambrian Research*, 122: 311–327.
Wu, F.Y., Sun, D.Y., Ge, W.C., Zhang, Y.B., Grant, M.L., Wilde, S.A., and Jahn, B.M., 2011. Geochronology of the Phanerozoic granitoids in northeastern China. Journal of Asian Earth Sciences, 41: 1–30.
Wu, F.Y., Sun, D.Y., Li, H.M., Jahn, B.M., and Wilde, S.A., 2002. A–type granites in northeastern China: Age and geochemical constraints on their petrogenesis. *Chemical Geology*, 187: 143–173.
Wu, F.Y., Yang, J.H., Lo, C.H., Wilde, S.A., Sun, D.Y., and Jahn, B.M., 2007a. The Heilongjiang Group: A Jurassic accretionary complex in the Jiamusi Massif at the western Pacific margin of northeastern China. Island Arc, 16: 156–172.
Xu, J.W., Zhu, G., Tong, W.X., Cui, K.R., and Liu, Q., 1987. Formation and evolution of the Tancheng–Lujiang wrench fault system: A major shear system to the northwest of the Pacific Ocean. Tectonophysics, 134: 273–310.
Xu, Z.Q., 1984. General of the Tancheng–Lujiang rift system. Collection Structure Geology, 3: 39–46 (in Chinese).
Yin, C.J, Peng, Y.J, Wang, Y.S., Li, R., and Chen, Y.J., 2005. New evidences of chronology of rift belt of Yitong–Shulan. Jilin Geology, 24: 6–15 (in Chinese with English abstract).
Yuan, H.L., Gao, S., Dai, M.N., Zong, C.L., Günther D., Fontaine, G.H., Liu, X.M., and Diwu, C.R., 2008. Simultaneous determinations of U–Pb age, Hf isotopes and trace element compositions of zircon by excimer laser–ablation quadrupole and multiple–collector ICP–MS. Chemical Geology, 247(1): 100–118.
Zhang, H., and Wang, X.F., 1995. The Evolution of the northern segment of Tan–Lu fault system in Mesozoic era. Shenyang: Memoirs of Shenyang Institute of Geology and Mineral Resources, (4): 50–77 (in Chinese with English with abstract).
Zhang, H., Yuan, H.L., Hu, Z.C., Liu, X.M., and Diwu, C.R., 2005. U–Pb zircon dating of the Mesozoic volcanic strata in Luanping of North Hebei and its significance. Earth Science, 30: 707– 720 (in Chinese with English abstract).
Zhang, H.H., Xu, Y.G., Ge, W.C., Ma, J.L., 2006. Geochemistry of late Mesozoic–Cenozoic basalts in Yitong–Datun area, Jilin Province and its implication. Acta Petrological Sinica, 22: 1579–1596 (in Chinese with English abstract).
Zhang, Q., Zhu, G., Liu, G.S., Teyssier, C., and Dunlapet, W.J., 2008. Sinistral transpressive deformation in the northern part of Zhangbaling uplift in the Tan–Lu fault zone and its ^{40}Ar /^{39}Ar dating. Earth Science Frontiers, 15(3): 234–249 (in Chinese with English abstract).
Zhang, Q.L., Wang, L.S., Xie, G.A., Du, J.M., Xu, S.Y., and Hu, X.Z., 2005. Discussion on Northward extension of Tanlu fault zone and its tectonic regime transformation. Geological Journal of China Universities, 11(40)**:** 577–584 (in Chinese with English with abstract).
Zhang, Y.Q., and Dong, S.W., 2008. Mesozoic tectonic evolution history of the Tan–Lu fault zone, China: Advances and new understanding. Geological Bulletin of China, 27(9): 1371–1390 (in Chinese with English abstract).
Zhang, Y.X., Sun, Y.S., Zhang, X.Z., and Yang, B.J., 1999. Manzhouli to Suifenhe of China Global geoscience transect (GGT). Beijing: Geological Publishing House, 31 (in Chinese with English with abstract).
Zhao, T., Zhu, G., Lin S.Z., and Wang, H.Q., 2016. Indentation–induced tearing of a subducting continent: Evidence from the Tan–Lu fault zone, East China. Earth–Science Reviews, 152: 14–36.
Zhao, Y., Yang, Z.Y., and Ma, X.H., 1994. Geotectonic transition from Paleoasian system and Paleotethyan system to Paleopacific active continental margin in Eastern Asia. Chinese Journal of Geology, 29(2): 105–119 (in Chinese with English abstract).
Zheng, Y.D., and Chang, Z.Z., 1985. Finite Strain Measurement and Ductile Shear Zones. Beijing: Geological Publishing House (in Chinese with English abstract).
Zhou, J.B., Zhang, X.Z., Wilde, S.A., Zheng, C.Q., Jin, W., Chen, H., and Han, J., 2009. Detrital zircon U–Pb dating of Heilongjiang complex and its tectonic implication. *Acta* Petrologica Sinica, 25(8): 1924–1936 (in Chinese with English with abstract).
Zhou, J.B., Wilde, S.A., Zhang, X.Z., Zhao, G.C., Zheng, C.Q., Wang, Y.J., Zhang, X.H., 2009a. The onset of Pacific margin accretion in NE China: Evidence from the Heilongjiang high–pressure metamorphic belt. *Tectonophysics*, 478: 230–246.
Zhou, Q., Wu, F.Y., Chu, Z.Y., Ge, W.C., 2010. Isotopic compositions of mantle xenoliths and age of the lithospheric mantle in Yitong, Jilin Province. Acta Petrological Sinica, 26: 1241–1264 (in Chinese with English abstract).
Zhu G, Niu M L, Xie C L, and Wang Y S. 2010. Sinistral to normal faulting along the Tan–Lu fault zone: Evidence for geodynamic switching of the East China continental margin. Journal of Geology, 118: 277–293
Zhu, G., Liou, G.S., Dunlap, W.J., Teyssier, C., W, Y.S., and Niu, M.L., 2004. $^{40}Ar–^{39}Ar$ geochronological constraints on syn–orogenic strke–slip movement of the Tan–Lu fault zone. Chinese Science Bulletin, 49(2): 190–198.
Zhu, G., Niu, M.L., Liu, G.S., Wang, D.X., and Song, C.Z., 2002. Structural, magmatic and sedimentary events of the Tan –Lu fault belt during its early Cretaceous strike–slip movement. Acta Geologica Sinica, 76(3): 325–334 (in Chinese with English with abstract).
Zhu, G., Song, C.Z., Wang, D.X., Liu G.S., and Xu, J.W., 2001. Studies on $^{40}Ar/^{39}Ar$ thermochronology of strke–slip time of the Tan–Lu fault zone and their tectonic implications. Science in China Series D: Earth Sciences, 44(11): 1002–1009.
Zhu, G., Wang, D.X., Liu, G.S., Niu, M.L., and Song, C.Z., 2004. Evolution of the Tan–Lu Fault Zone and its responses to plate movements in West Pacific Basin. Chinese Journal of Geology, 39: 36–49.
Zhu,G., Xie, C.L., Wang, Y.S., Niu, M.L., and Liou, G.S., 2005. Tan–Lu high–pressure strike–slip ductile shear zone and its $^{40}Ar/^{39}Ar$ dating. Acta Petrologica Sinica, 21(6): 1687–1702 (in Chinese with English with abstract).
Zhu. G., Liu, G.S., Niu, M.L., Song, C.Z., and Wang, D.X., 2003. Transcurrent movement and genesis of the Tan–Lu Fault Zone (in Chinese). Geological Bulletin of China, 22: 200–207 (in Chinese with English with abstract).

About the first author

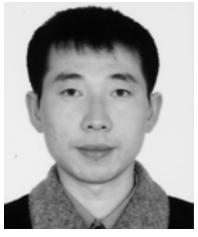

WEN Quanbo, male, born in 1978 in Changzhi City, Shanxi Province; lecturer; graduated from Jilin University; College of Earth Sciences, Jilin University. He is now interested in the study on structural geology, basic tectonics. Email: wenquanbo @163.com; phone: 13624316646.

About the corresponding author:

LIU Yongjiang, male, born in 1964 in Hailin City, Heilongjiang Province; professor; graduate from University of Salzburg; Ocean University of China. He is now interested in the study on structural geology, rheology and tectonics. Email: liuyongjiang@ouc.edu.cn; phone: 13844803058